AD-A111 198 NAVAL SURFACE WEAPONS CENTER SILVER SPRING MD F/G 20/7
FILAMENTATION INSTABILITY OF A RELATIVISTIC HOLLOW ELECTRON BEA--ETC(U)
SEP 81 H S UHM, J G SIAMBIS
UNCLASSIFIED NSWC/TR-81-385 NL

1 OF 1
AD A
111198

END
DATE
FILMED
03-82
DTIC

NSWC TR 81-385

(12)

AD A111198

FILAMENTATION INSTABILITY OF A RELATIVISTIC HOLLOW ELECTRON BEAM

BY HANS S. UHM J. G. SIAMBIS

RESEARCH AND TECHNOLOGY DEPT.

SEPTEMBER 1981

NAVAL SURFACE WEAPONS CENTER

Dahlgren, Virginia 22448 • Silver Spring, Maryland 20910

82 02 22 038

UNCLASSIFIED

SECURITY CLASSIFICATION OF THIS PAGE (When Data Entered)

REPORT DOCUMENTATION PAGE		READ INSTRUCTIONS BEFORE COMPLETING FORM
1. REPORT NUMBER NSWC TR 81-385	2. GOVT ACCESSION NO. AD-A111198	3. RECIPIENT'S CATALOG NUMBER
4. TITLE (and Subtitle) Filamentation Instability of a Relativistic Hollow Electron Beam		5. TYPE OF REPORT & PERIOD COVERED Final
		6. PERFORMING ORG. REPORT NUMBER
7. AUTHOR(s) J.G. Siambis and H.S. Uhm		8. CONTRACT OR GRANT NUMBER(s)
9. PERFORMING ORGANIZATION NAME AND ADDRESS Naval Surface Weapons Center R41 White Oak, Silver Spring, Maryland 20910		10. PROGRAM ELEMENT, PROJECT, TASK AREA & WORK UNIT NUMBERS 61152N, ZR00001, ZR01109, 0
11. CONTROLLING OFFICE NAME AND ADDRESS		12. REPORT DATE September 1981
		13. NUMBER OF PAGES 39
14. MONITORING AGENCY NAME & ADDRESS(if different from Controlling Office)		15. SECURITY CLASS. (of this report) UNCLASSIFIED
		15a. DECLASSIFICATION/DOWNGRADING SCHEDULE

16. DISTRIBUTION STATEMENT (of this Report)

Approved for public release, distribution unlimited

17. DISTRIBUTION STATEMENT (of the abstract entered in Block 20, if different from Report)

18. SUPPLEMENTARY NOTES

19. KEY WORDS (Continue on reverse side if necessary and identify by block number)

Hollow Electron Beam
Relativistic Particle
Filamentation Instability
Diocotron Instability

20. ABSTRACT (Continue on reverse side if necessary and identify by block number)

¬The filamentation instability properties of a relativistic hollow electron beam confined in axial flow by a uniform magnetic field in a pipe are investigated via the Vlasov-Maxwell equations. The instability is found to have two side-bands, one with a spectrum of positive wavenumbers k and the other with a spectrum of negative wavenumbers. The spectral point $k=0$, associated with the diokotron instability, is excluded from the filamentation instability's two unstable sidebands. Only in the limit of zero axial beam flow ($\gamma \rightarrow 1$), the diokotron instability becomes asymptotically part of the

filamentation instability spectrum. In this limit the filamentation instability's two sidebands merge asymptotically and symmetrically toward the diokotron instability spectral point, k=0, in agreement with the basic driving physical mechanisms and geometry configurations for these two distinct and different instabilities.

FOREWORD

The filamentation instability properties of a relativistic hollow electron beam confined in axial flow by a uniform magnetic field in a pipe are investigated via the Vlasov-Maxwell equations. The instability is found to have two sidebands, one with a spectrum of positive wavenumbers k and the other with a spectrum of negative wavenumbers. The spectral point k=0, associated with the diokotron instability, is excluded from the filamentation instability's two unstable sidebands. Only in the limit of zero axial beam flow ($\gamma \to 1$), the diokotron instability becomes asymptotically part of the filamentation instability spectrum. In this limit the filamentation instability's two sidebands merge asymptotically and symmetrically toward the diokotron instability spectral point, k=0, in agreement with the basic driving physical mechanisms and geometry configurations for these two distinct and different instabilities.

Ira M Blatstein

IRA M. BLATSTEIN
By direction

A

CONTENTS

ILLUSTRATIONS

ILLUSTRATIONS (Cont.)

INTRODUCTION

In a recent paper by Uhm and Siambis[1] the diokotron instability of a hollow relativistic electron beam in a conducting pipe guided by a uniform axial magnetic field was investigated. Relativistic and electromagnetic effects were included in the derivation of the properties of the instability. In Reference 1 the analysis of the diokotron modes proceeded by taking the limit k=0, ab initio, where k is the wave number along the beam. This restriction, of k=0, for the diokotron modes has been assumed in all earlier treatments of the diokotron instability[2-4]. Physically this assumption was motivated by the geometrical configuration of the magnetron tube[2] in particular, as well as other crossed field (E-cross-B) beam devices[3,5] utilizing hollow electron beams. Instabilities in hollow beams, in long cylindrical pipes, confined in axial flow by a uniform magnetic field, were investigated experimentally by Kyhl and Webster[6] and analytically by Pierce[7] in order to establish the mechanisms for noise generation and amplification in traveling wave microwave tubes with hollow beams. These early investigators[6,7] found that low voltage, low current hollow electron beams can break up into vortex filaments, similar to those associated with the diokotron instability, and in addition they exhibit a non-zero wave number, $k \neq 0$, along the applied magnetic field. They observed that the azimuthal wave length of the instability was comparable to the longitudinal wave length of the instability. They also observed that this comparability in axial and azimuthal wave lengths was maintained as the instability actually evolved from the fastest growing short wave lengths to the slower growing longer wave lengths. They called this instability the filamentation instability. These early investigators were interested in whether this phenomenon, at low levels, contributed to microwave tube beam noise. They concluded that a direct contribution to beam noise seemed unlikely since the waves did not have the proper symmetry to couple to the rf circuits of the microwave tubes[6]. This observation resulted in lack of broad further interest in this phenomenon.

More recently intense relativistic hollow electron beams have become the object of intense experimental and analytical investigations in connection with a broad spectrum of modern applications such as high current electron beam accelerators, collective accelerators, gyrotrons, free electron lasers and fusion. It is the purpose of this work to investigate the properties of the filamentation instability for intense, relativistic hollow electron beams of interest in current applications. In carrying out the analysis we shall follow the technique of Reference 8. In Section II the relativistic electron hollow beam equilibrium state is analysed. In Section III a Vlasov-Maxwell stability analysis is carried out. In Section IV the axisymmetric, $\ell=0$, space charge mode for the hollow beam is obtained and found to be in agreement with results from more approximate theories. In Section V the filamentation instability modes, $\ell \geqslant 3$, are analysed and discussed. In Section VI conclusions are presented.

EQUILIBRIUM

We consider the equilibrium configuration illustrated in Figure 1, consisting of an intense hollow relativistic electron beam propagating in a drift tube parallel to a uniform applied magnetic field, $B_0\hat{e}_z$, with velocity $\beta_b c\hat{e}_z$. Cylindrical coordinates (r,θ,z) are used, with the z axis along the axis of symmetry. The beam is described by a distribution $f(\vec{r},\vec{p},t)$ which satisfies the Vlasov equation

$$\left[\frac{\partial}{\partial t} + \vec{v}\cdot\vec{\nabla}_{\vec{r}} - e\left(\vec{E} + \frac{\vec{v}}{c}\times\vec{B}\right)\cdot\frac{\partial}{\partial\vec{p}}\right] f(\vec{r},\vec{p},t) = 0 \qquad (1)$$

where $\vec{r}$ stands for the cylindrical coordinates, the momentum $\vec{p}$ for p_r, p_θ, p_z, the fields $\vec{E}$ and $\vec{B}$ are the external and self-consistent fields associated with the beam flow. The velocity $\vec{v}$ is given by

$$\vec{v} = \vec{p}/\gamma m \quad , \qquad \beta = v/c \qquad (2)$$

where

$$\gamma = \left[1 + \frac{p^2}{m^2c^2}\right]^{\frac{1}{2}} \qquad (3)$$

and $-e$, m are the charge and rest mass of the electron, and c is the velocity of light.

The hollow beam equilibrium flow distribution, suitable for the application at hand, is given in terms of the constants of the motion.

$$f_b = \frac{n_0 R_0}{2\pi\gamma_b m}\ \delta(H - \beta_b c P_z - \gamma_0 mc^2/\gamma_b)\ \delta(P_\theta - P_0) \qquad (4)$$

where the total energy

$$H = (m^2c^4 + p^2c^4)^{\frac{1}{2}} - e\phi_0(r) \quad , \qquad (5)$$

the canonical angular momentum

$$P_\theta = r(p_\theta - \frac{1}{2}\frac{e}{c}B_o r) \quad , \tag{6}$$

and the axial cononical momentum

$$P_z = p_z - \frac{e}{c}A_z(r) \tag{7}$$

are the three single particle constants of the motion.

The constants n_o, R_o, P_o, γ_b and γ_o are identified as follows: The quantity n_o is the value of the density $n_b(r)$ at the median radius R_o as shown in Figure 2, P_o is the value of the canonical angular momentum at $r=R_o$, $\gamma_o mc^2$ is the total electron energy at the beam frame, and γ_b is given by

$$\gamma_b = (1 - \beta_b^2)^{-\frac{1}{2}} \quad . \tag{8}$$

We also define the energy variable U

$$U = H - \beta_b c P_z - \gamma_o mc^2/\gamma_b \tag{9}$$

and write the equilibrium distribution as

$$f_b = \frac{n_o R_o}{2\pi m\gamma_b}\,\delta(U)\delta(P_\theta - P_o) \quad . \tag{10}$$

After a straightforward algebra, U in Equation (9) is expressed as

$$U = \left\{\frac{\gamma' - \gamma_o}{\gamma_b}\ mc^2 - e\left[\phi_o(r) - \beta_b A_z(r)\right]\right\} \quad , \tag{11}$$

where $\gamma' mc^2$ is the electron kinetic energy at the beam frame.

The equilibrium electromagnetic fields are obtained from the scalar potential $\phi_o(r)$ and vector potential $A_z(r)$ from Maxwell's equations

$$\frac{1}{r}\frac{\partial}{\partial r} r \frac{\partial}{\partial r} \phi_o(r) = 4\pi e n_b(r) \tag{12}$$

$$\frac{1}{r}\frac{\partial}{\partial r} r \frac{\partial}{\partial r} A_z(r) = 4\pi e \beta_b n_b(r) \tag{13}$$

where $$n_b(r) = \int d^3p f_b(H, P_\theta, P_z) \quad , \tag{14}$$

which is found to be

$$n_b(r) = \begin{cases} 0 & , \; r < R_1 \\ n_o R_o / r & , \; R_1 < r < R_2 \\ 0 & , \; r > R_2 \end{cases} \quad . \tag{15}$$

Equations (12) - (15) give

$$E_r(r) = -\frac{\partial \phi_o(r)}{\partial r} = -4\pi e n_o R_o \,(1 - R_1/r) \quad , \quad R_1 < r < R_2 \tag{16}$$

$$B_\theta(r) = -\frac{\partial A_z(r)}{\partial r} = -4\pi e \beta_b n_o R_o \,(1 - R_1/r) \; , \quad R_1 < r < R_2 \quad . \tag{17}$$

The radial force balance on the beam electron field element, obtained from Equations (1) and (4), is

$$\frac{\gamma_b m V_\theta^2(r)}{r} = e\left[E_r(r) + \frac{V_\theta(r)}{c} B_o - \beta_b B_\theta(r)\right] \quad . \tag{18}$$

We define the equilibrium rotation frequency

$$\omega_e(r) = V_\theta(r)/r \tag{19}$$

and from Equation (18) write down its value for the median electron fluid element at $r=R_o$,

$$\omega_e(R_o) = \omega_e^{\pm}(R_o) \quad = \frac{\omega_c}{2}\left[1 \pm \left(1 - \frac{4\omega_{pb}^2}{\gamma_b^2\omega_c^2}\,\frac{a}{R_o}\right)^{\frac{1}{2}}\right]$$

where

$$\omega_c = \frac{eB_o}{mc\gamma_b} \quad , \tag{21}$$

$$\omega_{pb}^2 = \frac{4\pi e^2 n_b}{\gamma_b m} \quad , \tag{22}$$

and $a = R_2 - R_o = R_o - R_1$ is the half thickness of the hollow beam. The equilibrium state of interest is the one with the slow rotational frequency $\omega_e^-(R_o)$. Additional properties of the general equilibrium state, assumed here through Equation (11), are similar to those derived in Reference 8 for the non-relativistic case.

STABILITY ANALYSIS

In this section we use the linearized Vlasov-Maxwell equations to investigate the general normal modes ($\ell \geq 0$, $k \neq 0$) and their stability properties for the type of intense, hollow beams discussed in the equilibrium section. We adopt a normal mode approach in which all perturbed quantities are assumed to vary with r, θ, z, and t as

$$\delta\psi(\vec{r},t) = \delta\psi(r)\,\exp\left[i(\ell\theta + kz - \omega t)\right] \quad . \tag{23}$$

For the electromagnetic fields we assume the TM (transverse magnetic) modes which have the following field components

$$\delta\vec{E} = +\hat{e}_r\delta E_r + \hat{e}_\theta\delta E_\theta + \hat{e}_z\delta E_z \tag{24}$$

$$\delta\vec{B} = \hat{e}_r\delta B_r + \hat{e}_\theta\delta B_\theta \tag{25}$$

and which satisfy the linearized Maxwell's equations

$$\vec{\nabla}\cdot\delta\vec{E} = 4\pi\delta\rho \tag{26}$$

$$\vec{\nabla}\times\delta\vec{E} = \frac{i\omega}{c}\,\delta\vec{B} \tag{27}$$

$$\vec{\nabla}\times\delta\vec{B} = \frac{4\pi}{c}\,\delta\vec{J} - \frac{i\omega}{c}\,\delta\vec{E} \quad . \tag{28}$$

Sbustitution of Equation (28) into Equation (27) and rearrangement with Equation (26) generates the wave equation for δE_z

$$\left[\frac{1}{r}\frac{\partial}{\partial r}\,r\,\frac{\partial}{\partial r} - \frac{\ell^2}{r^2} - (k^2 - \omega^2/c^2)\right]\delta E_z = 4\pi i k\left(\delta\rho - \frac{\omega}{c^2 k}\,\delta J_z\right) \quad . \tag{29}$$

However, the axial component of the perturbed current density is approximated by

$$\delta J_z \approx \beta_b c \delta\rho \quad . \tag{30}$$

The analysis will now be restricted to the cases of interest, where $V_\theta/c << 1$ and

$$\omega_e^-(R_o) = \omega_{eo} \approx \frac{\omega_{pb}^2}{\gamma_b^2\omega_c} \frac{a}{R_o} \tag{31}$$

$$\omega \approx kv_b + \ell\omega_{eo} \tag{32}$$

$$\omega_s^2 = \omega_c^2 - \frac{\omega_{pb}^2}{\gamma_b^2}(1 + 2a/R_o) \tag{33}$$

$$\left|\frac{\omega - k\beta_b c - \ell\omega_{eo}}{\omega_s}\right|^2 \frac{a}{R_o} << 1 \quad . \tag{34}$$

With these assumptions the δJ_r and δJ_θ source terms in Equation (30) can be neglected. Also for wave numbers k satisfying

$$(k^2R_o^2/\gamma_b^2) << 1 \tag{35}$$

the third term in the left hand side of Equation (29) can be neglected, resulting in the approximate wave equation

$$\left[\frac{1}{r}\frac{\partial}{\partial r} r \frac{\partial}{\partial r} - \frac{\ell^2}{r^2}\right]\delta E_z = 4\pi ik\left(1 - \frac{\omega\beta_b}{kc}\right)\delta\rho \quad . \tag{36}$$

Next, the source term $\delta\rho$ will be evaluated by first finding the perturbation δf, of the distribution function f_b, from the linearized Vlasov equation

$$\delta f = e\int_{-\infty}^{t} dt' \exp(-i\omega t') \exp(ikz + i\ell\theta)\left[\delta\vec{E} + \frac{\vec{v}\times\delta\vec{B}}{c}\right]\frac{\partial}{\partial\vec{p}'} f_b \tag{37}$$

where the integration in t' is carried along the equilibrium particle trajectories. We integrate by parts with respect to t' and change variables to $\tau = t' - t$, to find

$$ik\delta f = e\left\{\delta E_z(r)\frac{\partial f_b}{\partial U} + i\left[(\omega - k\beta_b c)\frac{\partial f_b}{\partial U} + \ell\frac{\partial f_b}{\partial P_\theta}\right]I\right\} \tag{38}$$

where the orbit integral I is defined by

$$I = \int_{-\infty}^{0} d\tau\,\delta E_z(r')\exp\left[-i\omega\tau + i\ell(\theta' - \theta) + ik(z' - z)\right] \quad . \tag{39}$$

In order to evaluate Equations (37) - (39), we use

$$\dot{\theta}' = \omega_{eo} - \mu\frac{(P_\theta - P_o)}{\gamma_b m R_o^2} \tag{40}$$

$$\mu = \omega_o^2/\omega_s^2 - 1 \tag{41}$$

$$\omega_o^2 = \left(\frac{2P_o}{\gamma_b m R_o}\right)^2 = \omega_c^2\left(1 - \frac{4\omega_{pb}^2 a}{\gamma_b^2\omega_c^2 R_o}\right) \quad . \tag{42}$$

We assume that $\ell\,(\omega_c/\omega_s) \ll R_o/a$ and we approximate δE by

$$\delta E_z(r') = \delta E_z(R_o) + \frac{P_\theta - P_o}{\gamma_b m R_o}\frac{\omega_o}{\omega_s^2}\left(\frac{\partial\delta E_z}{\partial r}\right)_{R_o} \tag{43}$$

so that

$$I = i\left[\delta E_z(R_o) + \frac{P_\theta - P_o}{\gamma_b m R_o}\frac{\omega_o}{\omega_s^2}\left(\frac{\partial\delta E_z}{\partial r}\right)_{R_o}\right]\left[\omega - k\beta_c c - \ell\left(\omega_{eo} - \mu\frac{P_\theta - P_o}{\gamma_b m R_o^2}\right) - \frac{kp_z'}{\gamma_b^2 m}\right]^{-1} \tag{44}$$

where

$$p_z' = \frac{1}{\gamma_b}(p_z - \gamma_b m\beta_b c) \quad . \tag{45}$$

Next the charge perturbation $\delta\rho$ is obtained by carrying out the momentum space integration

$$\delta\rho = -e\int\delta f\, d^3p \tag{46}$$

to find the final approximate form of the wave equation

$$\left(\frac{1}{r}\frac{\partial}{\partial r}r\frac{\partial}{\partial r}-\frac{\ell^2}{r^2}\right)\delta E_z =$$

$$\frac{R_o}{a}\frac{\omega_{pb}^2}{\omega_s^2}\left(1-\frac{\omega\beta_b}{kc}\right)\left[\delta E_z(r)-\delta E_z(R_o)-\frac{\ell\omega_o}{\Omega}\left(\frac{r-R_o}{R_o}\right)\delta E_z(R_o)\right]$$

$$\times\left[\frac{\delta(r-R_o+a)}{r}+\frac{\delta(r-R_o-a)}{r}\right]+\omega_{pb}^2\frac{R_o}{r}\oplus\left[a^2-(r-R_o)^2\right]$$

$$\times\left(1-\frac{\omega\beta_b}{kc}\right)\left[-\frac{k^2}{\gamma_b^2}\frac{\delta E_z(R_o)}{\Omega^2}+\frac{\mu\ell^2}{R_o^2}\frac{\delta E_z(R_o)}{\Omega^2}-\frac{\ell\omega_o}{R_o\omega_s^2}\left(\frac{\partial\delta E_z}{\partial r}\right)_{R_o}\frac{1}{\Omega}\right] \quad (47)$$

where

$$\Omega = \omega - \ell\omega_{eo} - k\beta_b c \quad (48)$$

and $\oplus(x)$ in the Heavyside step function

$$\oplus(x) = \begin{cases} 1\ , & x \geqslant 0 \\ 0\ , & x < 0 \end{cases} \quad . \quad (49)$$

Having found an expression for $\delta\rho$ we can now check the validity of Equation (30), which equivalently neglects the δJ_r and δJ_θ contributions. The δJ_r contribution is of order

$$\left(\frac{a}{R_o}\right)\left(\frac{\Omega}{\omega_s}\right)^2 << 1 \quad (50)$$

and the δJ_θ contribution is of order

$$\frac{\ell v_\theta}{c} << 1 \quad . \quad (51)$$

THE ℓ=0 CASE

We shall first evaluate the $\ell=0$ case, which should reproduce the well known symmetric space charge waves of the hollow beam. The wave equation reduces to,

$$\frac{1}{r}\frac{\partial}{\partial r} r \frac{\partial}{\partial r}\,\delta E_z = S\left[\delta E_z(r) - \delta E_z(R_0)\right]\left[\frac{\delta(r - R_0 + a)}{r} + \frac{\delta(r - R_0 - a)}{r}\right]$$
$$- N\,\frac{R_0}{r}\,\delta E_z(R_0) \oplus \left|a^2 - (r - R_0)^2\right| \quad . \tag{52}$$

We solve this equation by following the steps from Equation (88) to Equation (99) of Reference 8 to find

$$\left[1 - S\ln\left(\frac{R_1R_2}{R_c^2}\right) + S^2\ln\left(\frac{R_2}{R_c}\right)\ln\left(\frac{R_1}{R_2}\right)\right](1 + N)$$
$$-\left\{\left[1 - S\ln\left(\frac{R_2}{R_c}\right)\right]\ln\left(\frac{R_0}{R_c}\right) + S\left[\ln\left(\frac{R_2}{R_c}\right)\right]^2\right\}\alpha_1$$
$$-\left\{\left[1 - S\ln\left(\frac{R_1}{R_c}\right)\right] + S\ln\left(\frac{R_0}{R_c}\right)\right\}\alpha_2 = 0 \tag{53}$$

where

$$S = \frac{R_0}{a}\,\frac{\omega_{pb}^2}{\omega_s^2}\left(1 - \frac{\omega\beta_b}{kc}\right) \tag{54}$$

$$N = \frac{\omega_{pb}^2}{\gamma_b^2}\left(1 - \frac{\omega\beta_b}{kc}\right)\frac{k^2}{\Omega^2} \tag{55}$$

$$\alpha_1 = (1 - S)\,N\,\frac{R_1}{R_0} - S \tag{56}$$

$$\alpha_2 = \left(1 - \ln\frac{R_2}{R_c}\right)N\,\frac{R_2}{R_0} - S\ln\frac{R_2}{R_c} - S\ln\frac{R_2}{R_c}\,N\,\frac{R_2}{R_0} \quad . \tag{57}$$

After Taylor expansion of Equation (53), we find

$$(\omega - k\beta_b c)^2 = \frac{2\nu}{\gamma_b^3} \frac{1 + \frac{3}{2}\varepsilon + \frac{1}{2}\varepsilon^2}{1 + \varepsilon} kc(kc - \omega\beta_b) \ln \frac{R_c}{R_2} \tag{58}$$

where

$$\varepsilon = \frac{\omega_{pb}^2}{\omega_s^2}\left(1 - \frac{\omega\beta_b}{kc}\right) \tag{59}$$

and ν is Budker's parameter defined by

$$\nu = \frac{4\pi R_o a n_b e^2}{mc^2} \tag{60}$$

and $N_b = 4\pi R_o a n_b$ is the number of particles per unit axial length.

When $\varepsilon \to 0$, then Equation (58) reduces to

$$(\omega - k\beta_b c)^2 = \frac{2\nu}{\gamma_b^3} (k^2c^2 - \omega^2) \ln \frac{R_c}{R_2} \tag{61}$$

which is identical to the result obtained by Briggs[9] for the hollow beam and solid beam space charge waves. In obtaining Equation (61), use has been made of the approximation $\omega \simeq \kappa\beta_b c$.

THE $\ell \neq 0$ CASE

We solve Equation (47) for the general case of $\ell \neq 0$ by following the steps from Equation (88) to Equation (99) of Reference 8. In order to keep the size and form of the resulting algebraic eigenvalue solution short and simple, we utilize first the following notation:

$$S_1 = \frac{R_o}{a}\frac{\omega_{pb}^2}{\omega_s^2}\left(1 - \frac{\omega\beta_b}{kc}\right) \tag{62}$$

$$S_2 = -\frac{\omega_{pb}^2}{\omega_s^2}\left(1 - \frac{\omega\beta_b}{kc}\right)\frac{\ell\omega_o}{\Omega} \tag{63}$$

$$N_1 = \frac{\omega_{pb}^2\left(1 - \frac{\omega\beta_b}{kc}\right)\ell^2}{\Omega^2(\ell^2 - 1)}\left(\mu - \frac{k^2R_o^2}{\ell^2\gamma_b^2}\right) \tag{64}$$

$$N_2 = -\frac{\ell\omega_o}{\Omega}\frac{\omega_{pb}^2\left(1 - \frac{\omega\beta_b}{kc}\right)}{\omega_s^2(\ell^2 - 1)} \quad . \tag{65}$$

The eigenvalue solution becomes

$$\begin{aligned}
&\left\{4\ell^2 g_f + 2\ell S_1 + 2\ell S_1\left(\frac{R_1}{R_2}\right)^{2\ell} + (2\ell g_f + S_1)\, S_1\left[1 - \left(\frac{R_1}{R_2}\right)^{2\ell}\right]\right\} \\
&\times(1 + N_1 + N_2) + (2\ell g_f + S_1)(X_1 - X_3)\left(\frac{R_1}{R_o}\right)^{\ell} - (2\ell + S_1)(X_2 + X_4)\left(\frac{R_o}{R_2}\right)^{\ell} \\
&+ S_1(X_2 - X_4)\left(\frac{R_1^2}{R_oR_2}\right)^{\ell} - \left[2\ell(g_f - 1) + S_1(X_1 + X_3)\right]\left(\frac{R_1R_o}{R_2^2}\right)^{\ell} \\
&+ 2\ell N_2\left(\frac{R_1}{R_2}\right)^{\ell}\left[\left(\frac{R_1}{R_o}\right)(1 - \ell - S_1)(S_1 - S_2) + \left(\frac{R_2}{R_o}\right)(1 - \ell + 2\ell g_f + S_1)\right. \\
&\left.\times (S_1 + S_2)\right] = 0
\end{aligned} \tag{66}$$

where

$$X_1 = \frac{R_1}{R_o}(1 - \ell - S_1)N_1 - (S_1 + S_2)(1 + N_2) \tag{67}$$

$$X_2 = \frac{R_2}{R_o}(1 - \ell + 2\ell g_f + S_1)N_1 + (S_1 - S_2)(1 + N_2) \tag{68}$$

$$X_3 = \left[\frac{R_1}{R_o}(1 - \ell - S_1) + S_1 + S_2\right]\ell N_2 \tag{69}$$

$$X_4 = \left[\frac{R_2}{R_o}(1 - \ell + 2\ell g_f + S_1) - S_1 + S_2\right]\ell N_2 \tag{70}$$

and

$$g_f = \left[1 - (R_2/R_c)^{2\ell}\right]^{-1} \quad . \tag{71}$$

Next, we Taylor expand Equation (66), following the approach of Equation (101) of Reference 8, to find

$$\Gamma_1 + \Gamma_2 \frac{\omega_{pb}^2}{\omega_s^2}\frac{\omega_o}{\Omega}\frac{a}{R_o}\varepsilon_o + \Gamma_3 \frac{\omega_{pb}^2}{\Omega^2}\frac{\ell a}{R_o}\varepsilon_o = 0 \tag{72}$$

where

$$\Gamma_1 = g_f\left(1 + \frac{\omega_{pb}^2}{\omega_s^2}\varepsilon_o\right) \tag{73}$$

$$\Gamma_2 = \ell\left(2 + \frac{\omega_{pb}^2}{\omega_s^2}\varepsilon_o\right)(g_f - 1) - \frac{\omega_{pb}^2}{2\omega_s^2}\varepsilon_o \tag{74}$$

$$\begin{aligned}\Gamma_3 = {} & \left(\mu - \frac{k^2R_o^2}{\ell^2\gamma_b^2}\right)\left[1 - \frac{\ell a}{2R_o} + \frac{3}{2}\frac{\omega_{pb}^2}{\omega_s^2}\left(1 - \frac{4\ell a}{3R_o}\right)\varepsilon_o + \frac{1}{2}\frac{\omega_{pb}^4}{\omega_s^4}\varepsilon_o^2\left(1 - \frac{2\ell a}{R_o}\right)\right] \\ & - \frac{\omega_o^2}{\omega_s^2}\left[\frac{\omega_{pb}^2}{\omega_s^2}\left(1 - \frac{3\ell a}{2R_o}\right)\varepsilon_o + \frac{\omega_{pb}^4}{2\omega_s^4}\left(1 - \frac{2\ell a}{R_o}\right)\varepsilon_o^2\right]\end{aligned} \tag{75}$$

$$\varepsilon_o = 1 - \frac{\omega\beta_b}{kc} \quad . \tag{76}$$

In the limit of lower intensity beam current satisfying $\omega_{pb}^2 \leqslant \omega_c^2$, the dispersion relation of Equation (72) simplifies to

$$g_f + 2\ell(g_f - 1)\frac{\omega_{pb}^2}{\omega_s^2}\varepsilon_o\frac{\omega_o}{\Omega}\frac{a}{R_o} + \frac{\omega_{pb}^2}{\Omega^2}\varepsilon_o\frac{\ell a}{R_o}\left[\frac{\omega_{pb}^2}{\omega_s^2\gamma_b^2}(\ell - 2)\frac{a}{R_o} - \frac{k^2R_o^2}{\gamma_b^2\ell^2}\right] = 0 \quad . \tag{77}$$

Equation (77) is the final form of the dispersion relation for the modes of interest. It has been solved numerically for the growth rate $\Omega_i = \mathrm{Im}\,\Omega$ and the Doppler-shifted real oscillation frequency $\Omega_r = \mathrm{Re}\,\Omega$, where $\Omega = \omega - k\beta_b c - \ell\omega_{eo}$, for a broad range of system parameters, γ_b, ω_{pb}/ω_c, $\omega_{pb}R_o/c$, a/R_o and R_o/R_c. Typical solutions are shown in Figures 3 for $\gamma_b = 1.1$ and 4 for $\gamma_b = 3$. First of all we note that for azimuthal mode numbers $\ell = 0$, 1, and 2 the solution of the dispersion relation of Equation (77) gives only stable waves. Unstables modes appear for $\ell \geqslant 3$ as shown in Figures 3 and 4. Several points are noteworthy in Figures 3 and 4. First, and contrary to all previous studies of the diokotron instability, we observe that as $k \to 0$ the diokotron instability disappears and is replaced by two fast waves. For low γ beams, Figure 3, we note that the well known filamentation instability occurs at small, but non-zero wavenumber k, it has a spectrum in k space which is nearly symmetric about the k=0 point, and excludes the k=0 point. The doppler shifted frequency of oscillation, given by

$$\Omega_r = \omega_r - k\beta_b c - \ell\frac{a}{R_o}\,\frac{\omega_{pb}^2}{\gamma_b^2\omega_c} \tag{78}$$

is constant, to lowest order, within the spectrum of instability for low γ beams, $\gamma \to 1$, while the instability growth rate decreases away from the maximum occurring near the $k \to \pm 0$ points. Both the growth rate and k-space spectral width of the instability increase with the azimuthal mode number ℓ. The real frequency ω_r also increases with ℓ. For higher γ beams (Figure 4, $\gamma_b = 3$) we find that the lowest order symmetry about the k=0 point, that was observed in Figure 3 for $\gamma_b = 1.1$, now disappears. We note in comparing Figures 3 and 4 that the growth rate and the doppler-shifted real frequency decrease when the γ of the beam increases.

Figure 5 shows the effect of varying the applied magnetic field in controlling the instability. For the positive k part of the instability spectrum we note that both the growth rate and spectral width decrease with increasing applied magnetic field while there also occurs a shift of the spectrum to longer wavelengths.

Figure 6 illustrates the dependence of the growth rate on the beam energy γ_b, over the positive k spectrum of instability, for the indicated parameters. The growth rate of the instability is monotonically reduced by increasing the beam energy. On Figure 6 we define the parameters ζ_0, ζ_m and Ω_i^m for convenience in further analysis and discussion. The symbol ζ_0 stands for the long wavelength cutoff limit of the instability positive k spectrum and the pair of symbols Ω_i^m/ω_{pb}, ζ_m stand for the value and associated wave number of maximum growth rate. Figure 7a shows the variation of ζ_0 and ζ_m with γ_b and Figure 7b shows the variation of Ω_i^m/ω_{pb} with γ_b for the indicated parameters. The wave numbers ζ_0 and ζ_m increase sharply for $\gamma_b \gtrsim 1$ and quickly saturate to their asymptotic values for $\gamma_b \gtrsim 1.5$. After a careful examination of Equations (76) and (77) we find analytically that the asymptotic value of ζ_0 is given by

$$\zeta_0 = \frac{k_0 c}{\omega_{pb}} \simeq \ell \beta_b \frac{\omega_{pb}}{\omega_c} \frac{a}{R_0} \quad . \tag{79}$$

Figure 7b shows that

$$\Omega_i^m \backsim 1/\gamma_b^2 \tag{80}$$

in agreement with the basic scaling for the diokotron mode obtained by Uhm and Siambis in Reference 1.

DISCUSSION AND CONCLUSIONS

We have carried out an extensive analysis of the filamentation instability of hollow beams which for the first time provides a detailed analytical understanding of the spectacular experimental results obtained by Kyhl and Webster[6] 26 years ago. The analytical results from this work for the filamentation instability when compared to our results for the diokotron instability in Reference 1 show that the two instabilities are very different in their detailed properties and that the diokotron instability ($k=0$) is not a limiting case of the filamentation instability when $k \to 0$, despite the fact that the physical mechanisms for the two instabilities are of a similar nature, namely the azimuthal drift of the electrons and the hollowness of the radial density profile. This is understandable given the different physical situations where each of the two instabilities was first observed. The diokotron instability was first found by Buneman[2,5] in 1944 as an explanation for magnetron start up. In France, Doehler, Warnecke and Mourier[5] supported E-cross-B flow between non-emitting electrodes and observed the diokotron instability. They called their device the "diokotron" because they realized the effect was due to velocity shear, i.e., the pursuit of electron layers of each other (διωκειν = pursue). The diokotron instability, therefore, found birth in cross-field devices, most prominent of which is the magnetron. In these devices the electron zero order motion is in the transverse (r,θ) plane, where the diokotron instability also takes place. The axial (z) direction in cross-field devices is basically an ignorable coordinate; it is often short and wave activity along it is suppressed by the axial boundary conditions of the beam and the confining cavity, hence the assumption of $k=0$ for the diokotron instability. This contrasts very sharply with the physical situation where the filamentation instability applies. Namely the case of a hollow beam in zero order axial flow having only a higher order azimuthal drift velocity resulting from cross-field forces. In this case wave motion along the zero order beam flow in the z-direction naturally plays a significant role; hence $k \neq 0$ and the filamentation instability has a spectrum in k-space, in fact two spectral bands, one for positive and one for negative k. It is interesting to

NSWC TR 81-385

note in Figures 3, 4, and 6 that as the beam's axially directed zero order motion decreases to zero ($\gamma_b \to 1$) then the beam's azimuthal drift velocity, resulting from cross-field forces, becomes more important and the filamentation instability asymptotically reaches and includes in a limiting sense (as $k \to 0$) the diokotron instability.

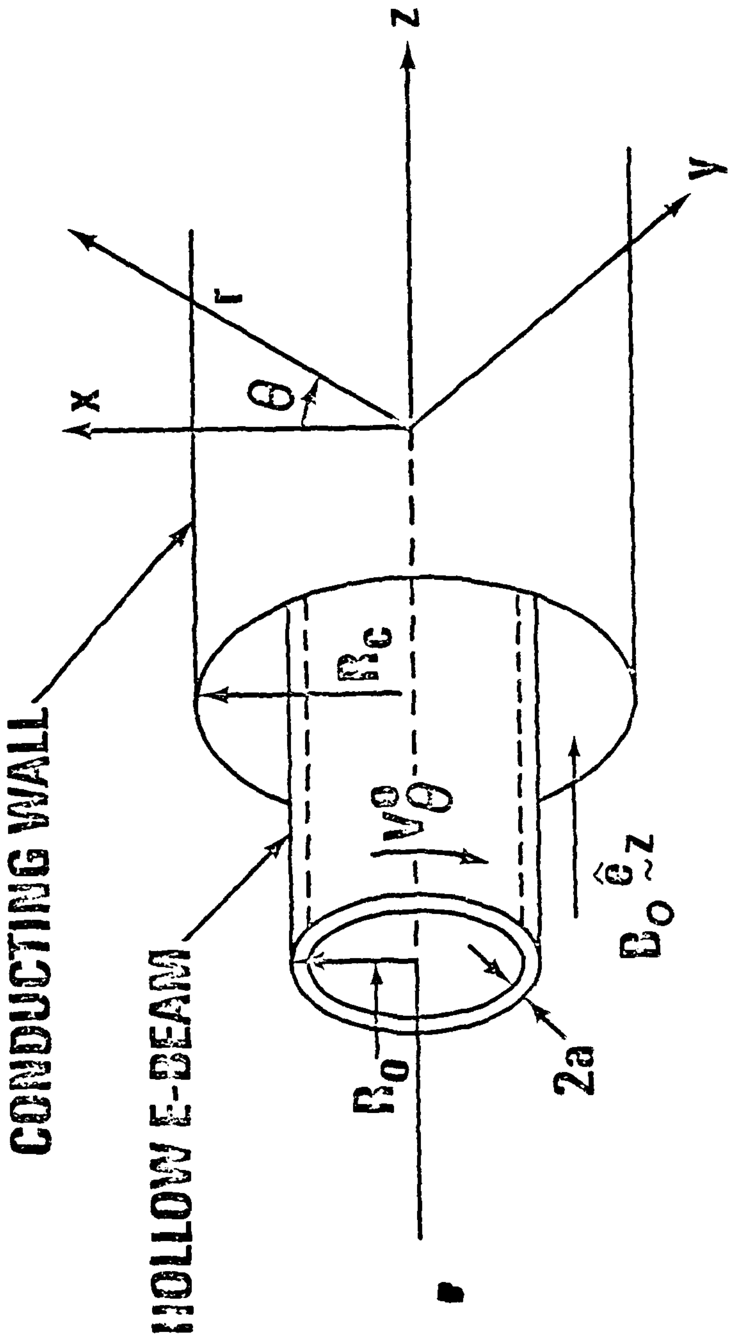

Fig. 1 Equilibrium configuration and coordinate system.

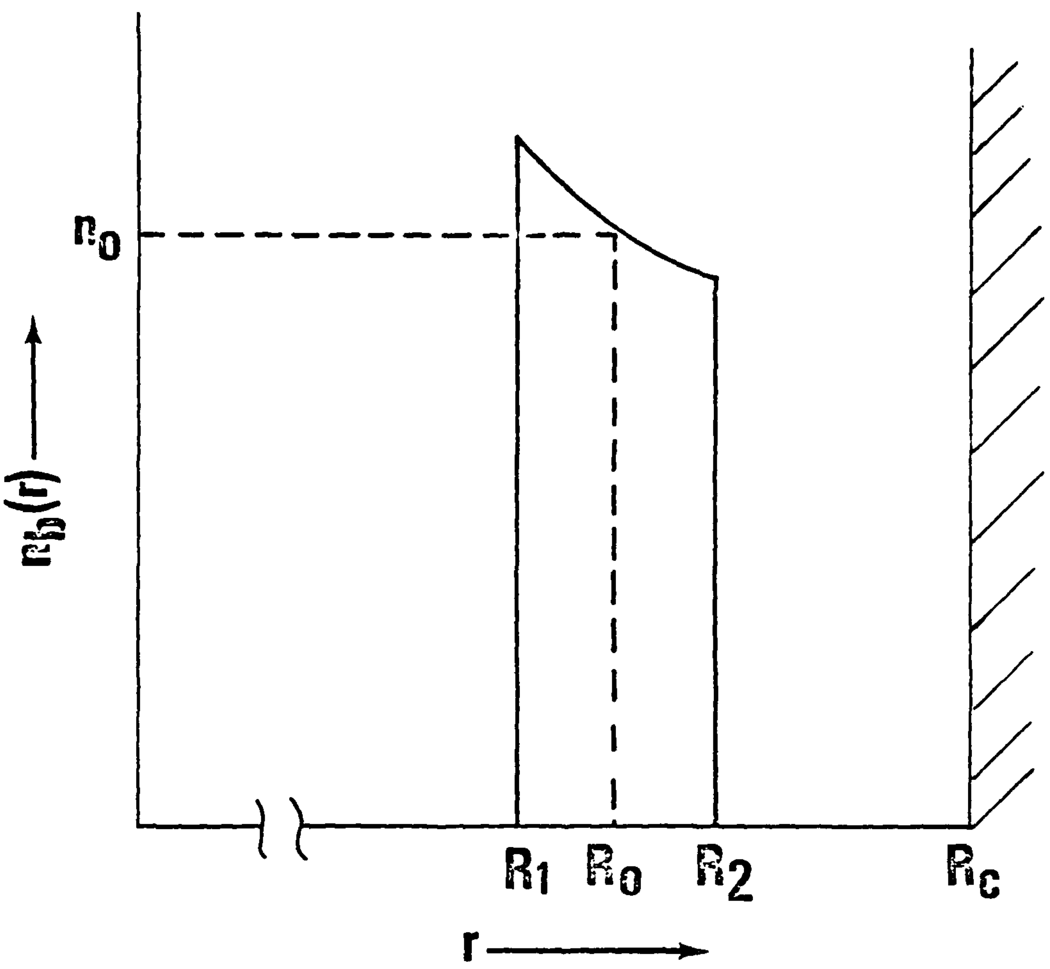

Fig. 2 Radial profile of beam density.

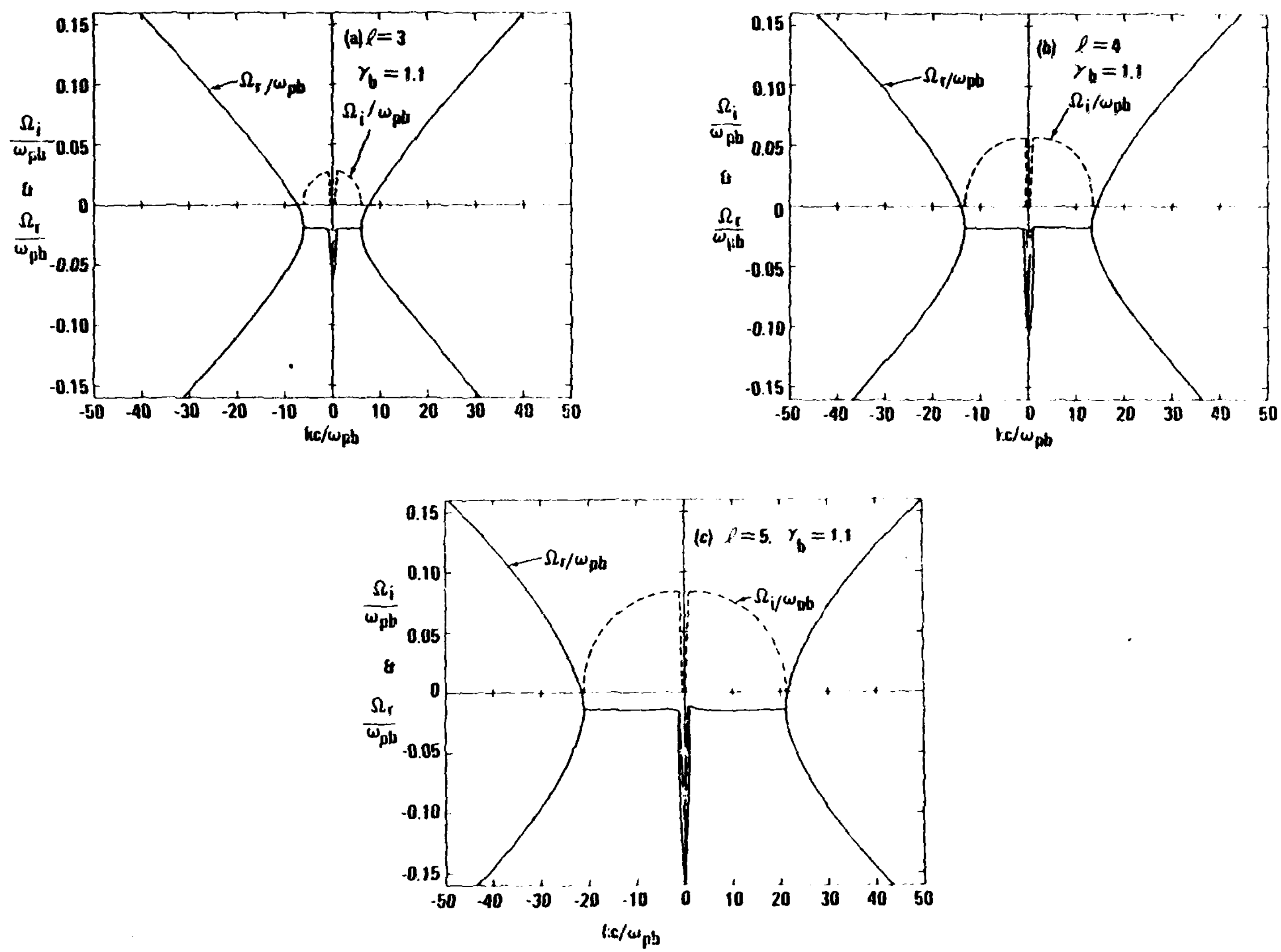

Fig. 3 Plots of normalized Doppler-shifted real frequency, Ω_r/ω_{pb} (solid curves), and normalized growth rate, Ω_i/ω_{pb} (dashed curve), versus normalized axial wavelength, kc/ω_{pb}, for three azimuthal mode numbers: (a) $\ell = 3$, (b) $\ell = 4$, (c) $\ell = 5$. The beam and geometry parameters are: $\gamma_b = 1.1$, $a/R_o = 0.05$, $R_o/R_c = 0.8$, $\omega_{pb}R_o/c = 0.05$, $\omega_{pb}/\omega_c = 0.5$.

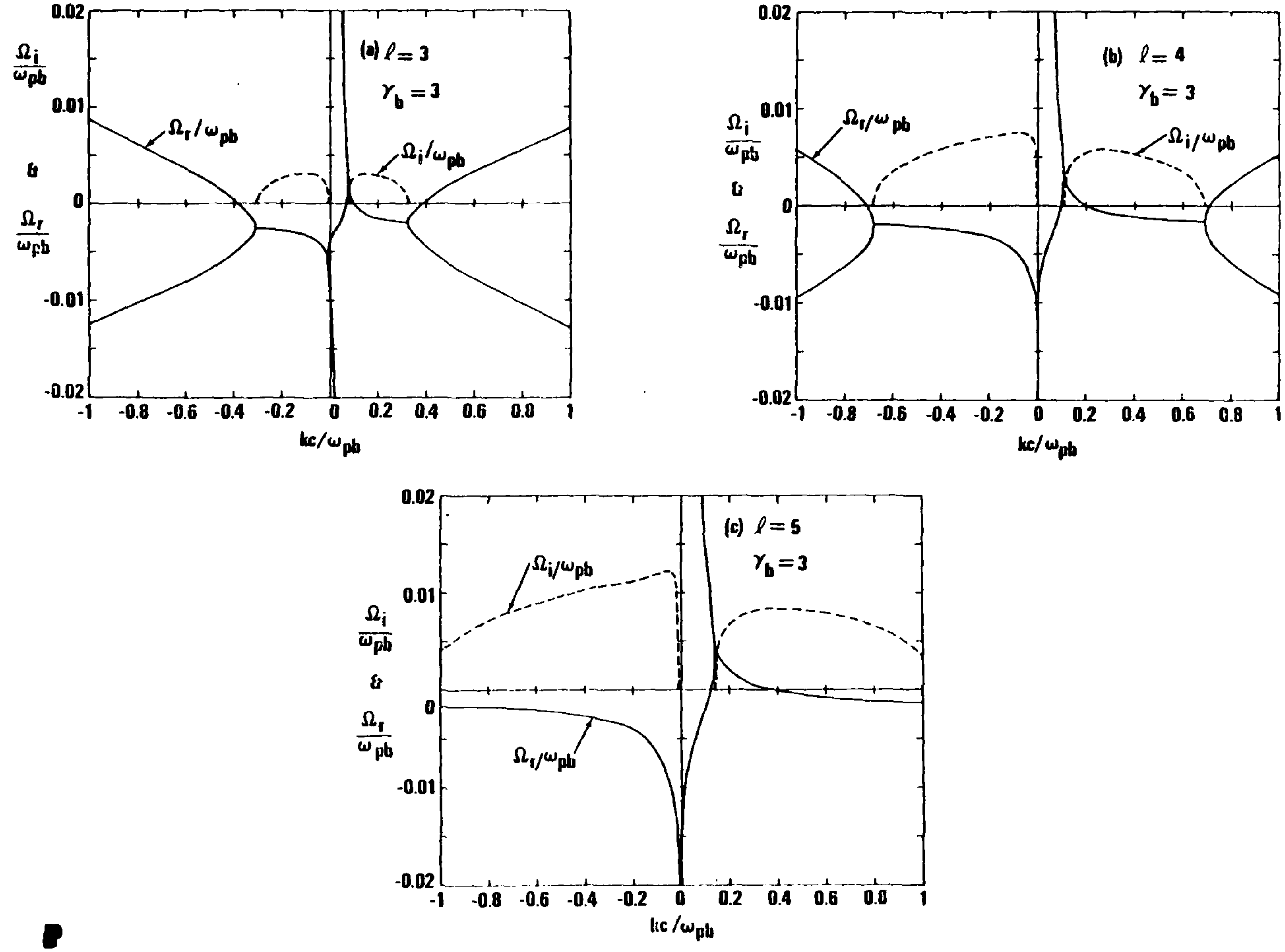

Fig. 4 Plots of normalized Doppler -shifted real frequency, Ω_r/ω_{pb} (solid curves), and normalized growth rate, Ω_i/ω_{pb} (dashed curve), versus normalized axial wavelength, kc/ω_{pb}, for three azimuthal mode numbers: (a) $\ell = 3$, (b) $\ell = 4$, (c) $\ell = 5$. The beam geometry parameters are: $\gamma_b = 3$, $a/R_o = 0.05$, $R_o/R_c = 0.8$, $\omega_{pb}R_o/c = 0.9$, $\omega_{pb}/\omega_c = 0.5$.

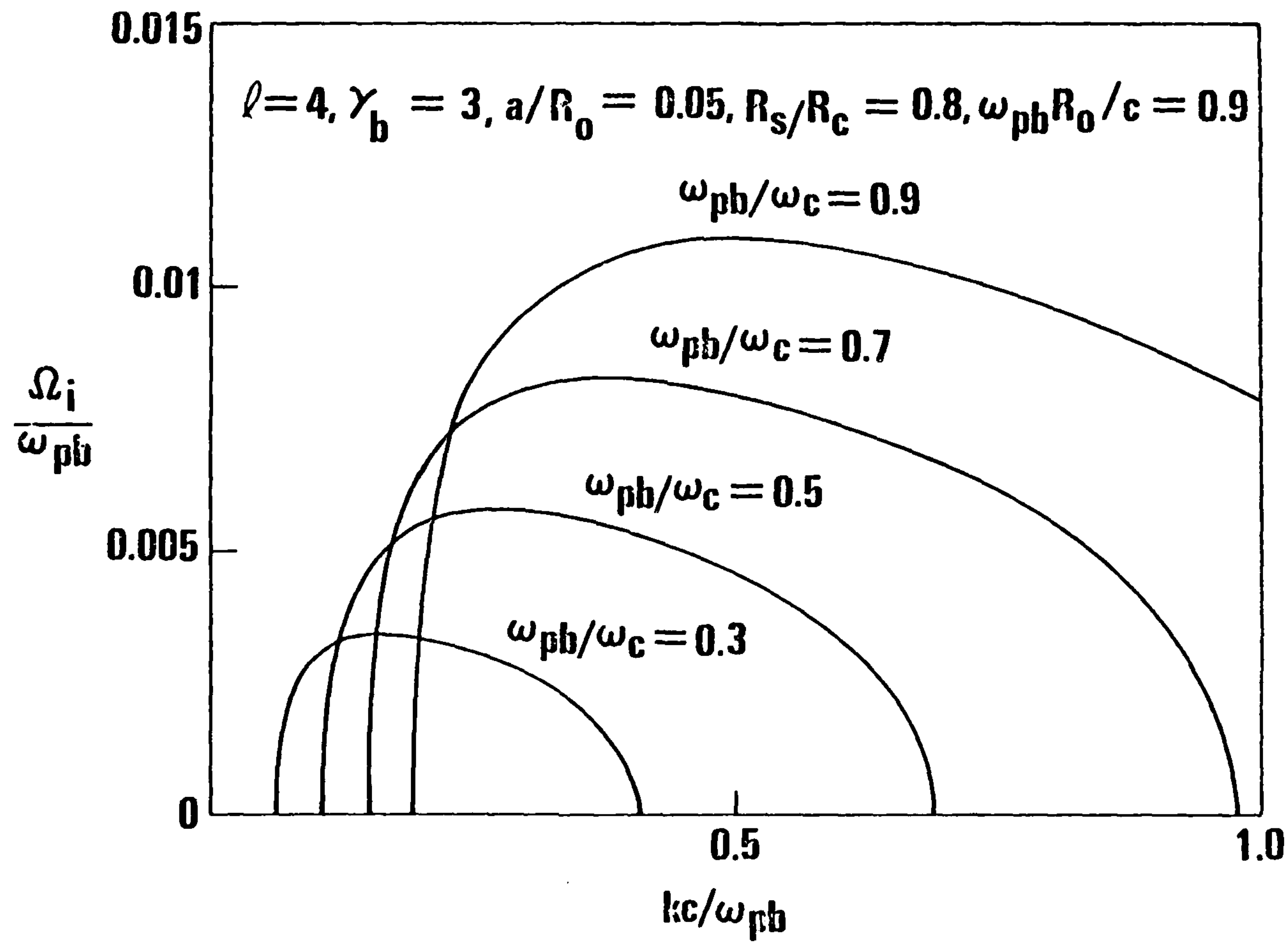

Fig. 5 Dependence of the growth rate and the positive k spectrum of the instability on the applied magnetic field via the parameter ω_{pb}/ω_c, for the case of $\ell = 4$, $\gamma_b = 3$, $a/R_o = 0.05$, $R_o/R_c = 0.8$, $\omega_{pb}R_o/c = 0.9$.

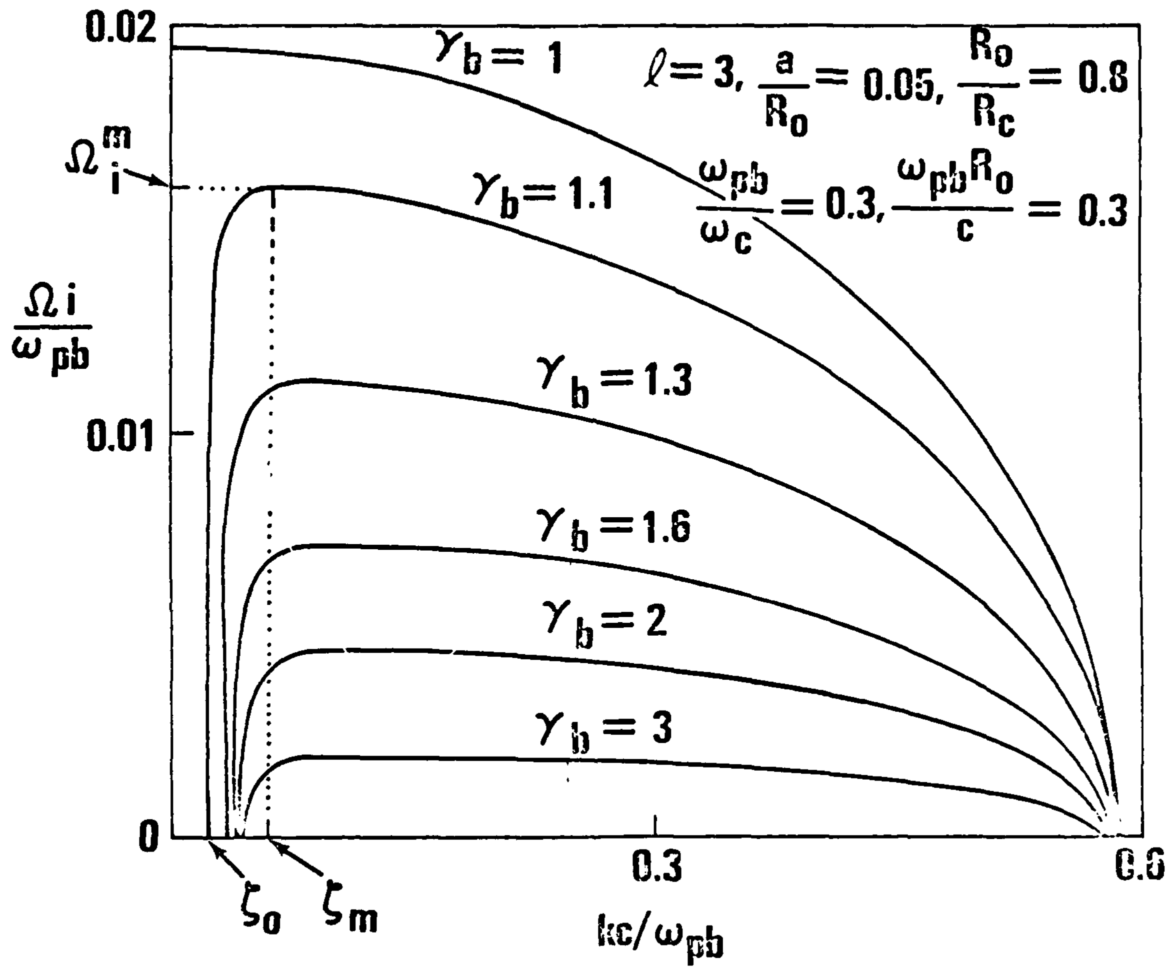

Fig. 6 Dependence of the growth rate and the long wavelength cutoff of the positive k spectrum of the instability on the beam energy γ_b, for the case of $\ell = 3$, $a/R_o = 0.05$, $R_o/R_c = 0.8$, $\omega_{pb}/\omega_c = 0.3$, $\omega_{pb}R_o/c = 0.3$. (Note that the latter two parameters are different from those in Figs. 3 - 5)

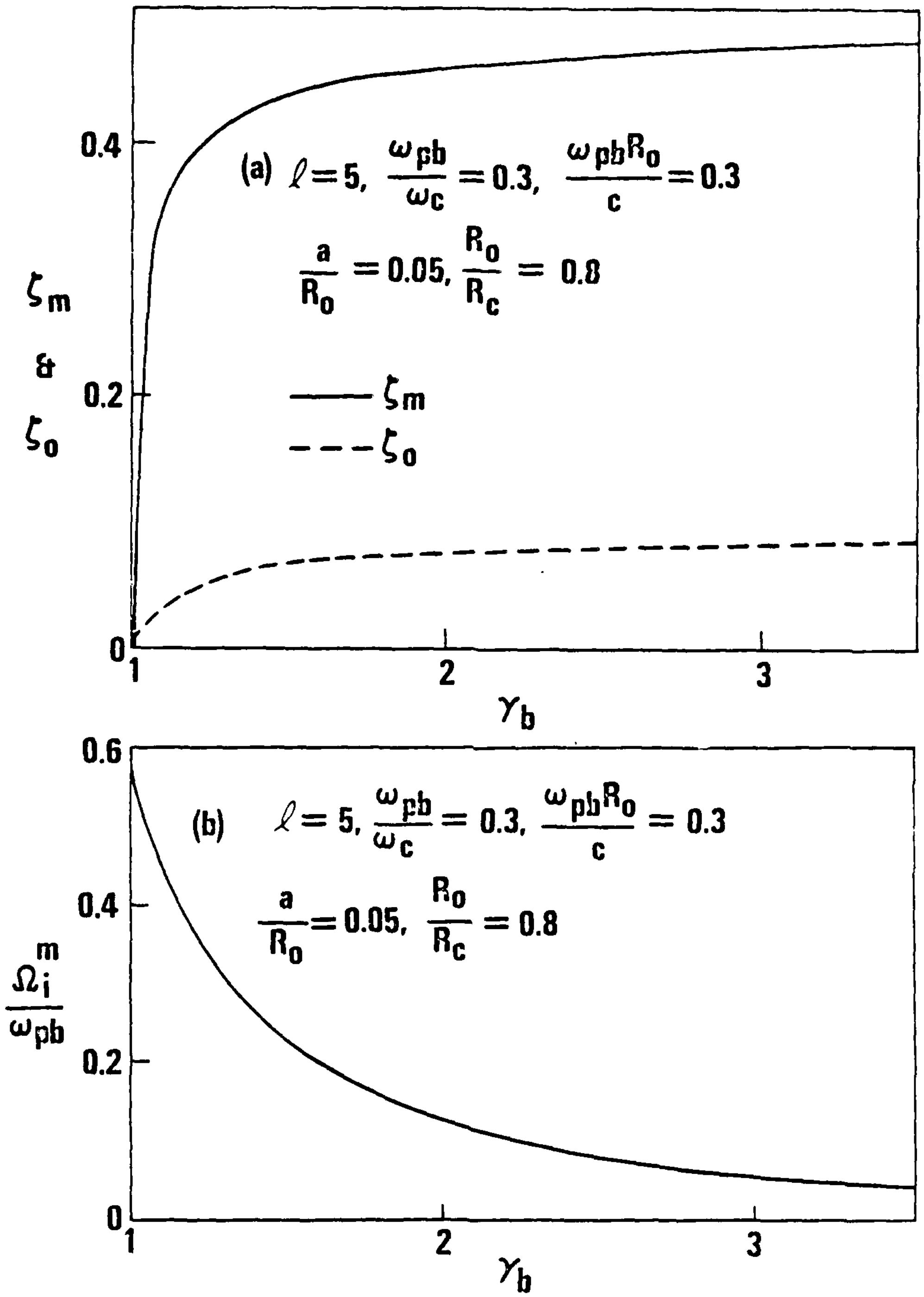

Fig. 7 Dependence of (a) long wavelength cutoff limit ζ_o and wave number for maximum growth ζ_m of the positive k spectrum of the instability on γ_b and (b) maximum growth rate Ω_i^m/ω_{pb} on γ_b. The parameters are $\ell = 5$, $a/R_o = 0.05$, $R_o/R_c = 0.8$, $\omega_{pb}R_o/c = 0.3$, $\omega_{pb}/\omega_c = 0.3$.

ACKNOWLEDGMENTS

The authors are indebted to O. Buneman, B. Epstein, M. Friedman, Bruce Miller and David Straw for useful discussions. The work of JGS was supported by the Office of Naval Research, the Department of Energy Office of Fusion Energy, Science Applications Inc., and Sandia National Laboratories. The work of HSU was supported by the Independent Research Fund at the Naval Surface Weapons Center.

REFERENCES

1. H.S. Uhm and J.G. Siambis, Phys. Fluids 22, 2377 (1979).
2. O. Buneman, J. Electronics and Control 3, 1 (1957).
3. R.H. Levy, Phys. Fluids 8, 1288 (1965).
4. C.A. Kapetanakos, D.A. Hammer, C.D. Striffler and R.C. Davidson, Phys. Rev. Lett. 30, 1303 (1973).
5. O. Buneman, private communication.
6. R.L. Kyhl and H.F. Webster, IRE Trans. Electron Devices ED-3, 172 (1956).
7. J.R. Pierce, IRE Trans. Electron Devices ED-3, 183 (1956).
8. R.C. Davidson, H.S. Uhm, and S.M. Mahajan, Phys. Fluids 19, 1608 (1976).
9. R.J. Briggs, Phys. Fluids 19, 1257 (1976).

DISTRIBUTION

	Copies
Commander	
Naval Research Laboratory	
Attn: Dr. Saeyoung Ahn	1
Dr. Wahab A. Ali	1
Dr. J. M. Baird	1
Dr. L. Barnett	1
Dr. O. Book	1
Dr. Jay Boris	1
Dr. K. R. Chu	1
Dr. Timothy Coffey	1
Dr. G. Cooperstein	1
Dr. A. Drobot	1
Dr. Richard Fernslor	1
Dr. H. Freund	1
Dr. M. Friedman	1
Dr. J. Golden	1
Dr. S. Goldstein	1
Dr. V. Granatstein	1
Dr. Robert Greig	1
Dr. Irving Haber	1
Dr. Richard Hubbard	1
Dr. Bertram Hui	1
Dr. Glenn Joyce	1
Dr. Selig Kainer	1
Dr. C. A. Kapetanakos	1
Dr. M. Lampe	1
Dr. Y. Y. Lau	1
Dr. W. M. Manheimer	1
Dr. Don Murphy	1
Dr. Peter Palmadesso	1
Dr. Robert Pechacek	1
Dr. Michael Picone	1
Dr. Michael Raleigh	1
Dr. M. E. Read	1
Dr. C. W. Roberson	1
Dr. J. D. Sethian	1
Dr. William Sharp	1
Dr. J. S. Silverstein	1
Dr. Philip Sprangle	1
Dr. Doug Strickland	1
Dr. C. M. Tang	1
Dr. N. Vanderplaats	1
Washington, DC 20375	

	Copies
Office of Naval Research	
Attn: Dr. Robert Behringer	1
1030 E. Green	
Pasadena, CA 91106	
Office of Naval Research	
Attn: Dr. T. Berlincourt	1
Dr. W. J. Condell	1
Department of the Navy	
Arlington, VA 22217	
Commander	
Naval Air Systems Command	
Attn: Dr. Wasneski	1
Department of the Navy	
Washington, DC 20361	
Commander	
Naval Sea Systems Command	
Attn: Dr. C. F. Sharn	1
Department of the Navy	
Washington, DC 20362	
Harry Diamond Laboratory	
Attn: Dr. H. E. Brandt	1
Dr. S. Graybill	1
2800 Powder Mill Road	
Adelphi, MD 20783	
U. S. Army Ballistic Research Laboratory	
Attn: Dr. D. Eccleshall	1
Aberdeen Proving Ground	
MD 21005	
Air Force Weapons Laboratory	
Attn: Dr. Ray Lemke	1
Kirtland Air Force Base	
Albuquerque, NM 87117	
Air Force Weapons Laboratory	
Attn: Dr. D. Straw	1
Kirtland AFB, NM 87117	

DISTRIBUTION (Cont.)

	Copies
U.S. Department of Energy	
Attn: Dr. T. Godlove	1
Dr. M. Month	1
Dr. J. A. Snow	1
Washington, DC 20545	
National Bureau of Standards	
Attn: Dr. Sam Penner	1
Bldg. 245	
Washington, DC 20234	
National Bureau of Standards	
Attn: Dr. Mark Wilson	1
Gaithersburg, MD 20760	
Defense Advanced Research Projects Agency	
Attn: Dr. J. Bayless	1
Dr. Robert Fossum	1
Dr. J. A. Mangano	1
LCOL W. Whitaker	1
1400 Wilson Blvd.	
Arlington, VA 22209	
Science Applications Inc.	
Attn: Dr. Richard E. Aamodt	1
934 Pearl St. Suite A	
Boulder, CO 80302	
Science Applications Inc.	
Attn: Dr. L. Feinstein	1
Dr. Robert Johnston	1
Dr. Douglas Keeley	1
Dr. John Siambis	1
5 Palo Alto Square	
Palo Alto, CA 94304	
Science Applications, Inc.	
Attn: Dr. A. W. Trivelpiece	1
San Diego, CA 92123	
Science Applications, Inc.	
Attn: Dr. Ron Parkinson	1
1200 Prospect Street	
P.O. Box 2351	
La Jolla, CA 92038	

	Copies
TRW	
Defense and Space Systems Group	
Attn: Dr. D. Arnush	1
Dr. M. Caponi	1
1 Space Park	
Redondo Beach, CA 90278	
Lawrence Livermore National Laboratory	
Attn: Dr. W. A. Barletta	1
Dr. R. Briggs	1
Dr. H. L. Buchanan	1
Dr. Frank Chambers	1
Dr. T. Fessenden	1
Dr. Edward P. Lee	1
Dr. James Mark	1
Dr. Jon A. Masamitsu	1
Dr. V. Kelvin Neil	1
Dr. R. Post	1
Dr. D. S. Prono	1
Dr. M. E. Rensink	1
Dr. Simon S. Yu	1
University of California	
Livermore, CA 94550	
Physics International Co.	
Attn: Dr. Jim Benford	1
Dr. S. Putnam	1
2700 Merced Street	
San Leandro, CA 94577	
Sandia Laboratories	
Attn: Dr. K. D. Bergeron	1
Dr. B. Epstein	1
Dr. S. Humphries	1
Dr. Tom Lockner	1
Dr. Bruce R. Miller	1
Dr. C. L. Olson	1
Dr. Gerold Yonas	1
Albuquerque, NM 87115	
La Jolla Institute	
Attn: Dr. K. Brueckner	1
Prof. N. M. Kroll	1
P.O. Box 1434	
La Jolla, CA 92038	

DISTRIBUTION (Cont.)

	Copies
Mission Research Corp.	
Attn: Dr. Neal Carron	1
Dr. Conrad Longmire	1
735 State Street	
Santa Barbara, CA 93102	
Mission Research Corp.	
Attn: Dr. B. Godfrey	1
1400 San Mateo Blvd, S.E.	
Suite A	
Albuquerque, NM 87108	
McDonnell Douglas Corp.	
Attn: Dr. M. Greenspan	1
Dr. J. Carl Leader	1
P. O. Box 516	
St. Louis, MO 63166	
Los Alamos National Lab.	
Attn: Dr. Barry Newberger	1
Dr. L. E. Thode	1
Mail Stop 608	
Los Alamos, NM 87544	
Los Alamos Scientific Lab.	
Attn: Dr. H. Dreicer	1
Dr. R. J. Faehl	1
Los Alamos, NM 87544	
Pulse Sciences, Inc.	
Attn: Dr. Sid Putnam	1
1615 Broadway, Suite 610	
Oakland, CA 94612	
National Science Foundation	
Attn: Dr. R. Hill	
Physics Division, #341	
Washington, DC 20550	
W. J. Schafer Associates, Inc.	
Attn: Dr. Edward Cornet	1
1901 North Fort Myer Dr.	
Arlington, VA 22209	

	Copies
Austin Research Associates	
Attn: Prof. W. E. Drummond	1
Dr. M. Lee Sloan	1
Dr. James R. Thompson	1
1901 Rutland Drive	
Austin, TX 78758	
Western Research Corporation	
Attn: Dr. Franklin Felber	1
8616 Commerce Avenue	
San Diego, CA 92121	
Jaycor	
Attn: Dr. J. U. Guillory	1
Dr. D. Tidman	1
205 S. Whiting Street	
Alexandria, VA 22304	
Varian Associates	
Attn: Dr. Howard Jory	1
611 Hansen Way	
Palo Alto, CA 94303	
Lawrence Berkeley Lab.	
Attn: Dr. Denis Keefe	1
Dr. Hogil Kim	1
Dr. Hong Chul Kim	1
Dr. Kwang Je Kim	1
Dr. L. J. Laslett	1
Dr. G. R. Lambertson	1
Dr. A. M. Sessler	1
Dr. L. Smith	1
1 Cyclotron Road	
Berkeley, CA 94720	
Stanford Linear Accelerator Center	
Attn: Dr. Philip Morton	1
P.O. Box 4349	
Stanford, CA 94305	
AVCO - Everett Research Laboratory, Inc.	
Attn: Dr. Richard Patrick	1
2385 Revere Beach Pkwy	
Everett, MA 02149	

DISTRIBUTION (Cont.)

	Copies
Oak Ridge National Lab	
Attn: Dr. J. A. Rome	1
Oak Ridge, TN 37850	
University of California at Los Angeles	
Attn: Prof. F. Chen	1
Dr. A. T. Lin	1
Dr. J. Dawson	1
Dr. C. S. Liu	1
Dr. Edward Ott	1
Los Angeles, CA 90024	
University of Maryland	
Attn: Dr. W. Destlar	1
Dr. C. S. Liu	1
Dr. Won Namkung	1
Dr. E. Ott	1
Prof. M. Reiser	1
Dr. Moon-Jhong Rhee	1
Dr. C. D. Striffler	1
College Park, MD 20742	
Columbia University	
Attn: Prof. P. Diament	1
Prof. S. Schlesinger	1
New York, NY 10027	
North Carolina State University	
Attn: Prof. W. Doggett	1
Dr. Jin Joong Kim	1
P. O. Box 5342	
Raleigh, NC 27650	
Massachusetts Institute of Technology	
Attn: Prof. George Bekefi	1
Dr. K. J. Button	1
Prof. R. Davidson	1
Dr. R. Temkin	1
77 Massachusetts Avenue	
Cambridge, MA 02139	
University of California	
Attn: Dr. Gregory Benford	1
Dr. A. Fisher	1
Prof. N. Rostoker	1
Physics Department	
Irvine, CA 92717	
Yale University	
Attn: Dr. I. B. Bernstein	1
Dr. J. L. Hirshfield	1
Mason Laboratory	
400 Temple Street	
New Haven, CT 06520	
Cornell University	
Attn: Prof. H. Fleischmann	1
Prof. D. Hammer	1
Prof. R. V. Lovelace	1
Prof. J. Nation	1
Prof. R. Sudan	1
Ithaca, NY 14850	
University of Texas at Austin	
Attn: Dr. M. N. Rosenbluth	1
Institute for Fusion Studies	
RLM 11.218	
Austin, TX 78712	
Stevens Institute of Technology	
Attn: Prof. George Schmidt	1
Physics Department	
Hoboken, NJ 07030	
Dartmouth College	
Attn: Dr. John E. Walsh	1
Department of Physics	
Hanover, NH 03755	
Defense Technical Information Center	
Cameron Station	
Alexandria, VA 22314	12

MED

8